Using Bessel Beams to Induce Optical Waveguides

Feifei Xin,[1,2] Mariano Flammini,[1] Fabrizio Di Mei,[1] Ludovica Falsi,[1,3] Davide Pierangeli,[1,4] Aharon J. Agranat,[5] and Eugenio DelRe[1,6,*]

[1] *Dipartimento di Fisica, Università di Roma "La Sapienza," Rome 00185, Italy*
[2] *College of Physics and Materials Science, Tianjin Normal University, Tianjin 300387, China*
[3] *Dipartimento S.B.A.I., Sezione di Fisica, Università di Roma "La Sapienza," Rome, 00161, Italy*
[4] *ICL-2DMOST, College of Optoelectronic Engineering, Shenzhen University, Shenzhen 518060, China*
[5] *The Brojde Center for Innovative Engineering and Computer Science, The Hebrew University, Jerusalem 91904, Israel*
[6] *ISC-CNR, Università di Roma "La Sapienza," Rome 00185, Italy*

(Received 10 October 2018; revised manuscript received 7 December 2018; published 5 February 2019)

Optical fabrication of waveguides in a volume is limited by diffraction in the writing beams. We demonstrate the use of nondiffracting waves in the form of Bessel beams to fabricate scalable optical wiring through direct writing in a photosensitive volume. Experiments are performed in paraelectric potassium-lithium-tantalate-niobate (KLTN), where writing occurs through photogenerated space charge while guiding and electro-optic functionality are supported by the quadratic electro-optic effect. The method allows components to be integrated sequentially without interfering with each other during fabrication, an intrinsic superposition property that is used to realize single, double, and multiple waveguides, and 1×2, 1×3, and 1×4 splitters, and electrically controlled optical switching.

DOI: 10.1103/PhysRevApplied.11.024011

I. INTRODUCTION

Programmable waveguides scalable into highly integrated photonic circuits are key ingredients in the development of innovative optical technology in various rapidly growing fields, including linear quantum computation and optical information processing [1]. While present achievements are based on planar photonic circuits [2–4], optical networks can in principle operate in a fully three-dimensional volume, thus increasing the achievable number of interlinked gates and devices. Operating in a volume requires specific fabrication tools, such as direct optical writing [5–10]. At present, direct writing involves a step-by-step fabrication that becomes increasingly cumbersome as design complexity grows. Furthermore, as the details of the circuitry are scaled down to the optical wavelength, diffraction in the writing beams limits the available volume, ultimately compromising scalability. Previous studies have attempted to overcome diffractive distortion in optical writing through nonlinear beam propagation, as occurs in self-writing and spatial solitons [11–15]. This process, however, causes optical writing to be dominated by light-light interaction, greatly complicating circuit design [16–19]. At present, no scalable optical writing technique based solely on linear waves has been demonstrated in a full macroscopic volume.

In this paper, we demonstrate a scalable method to optically induce waveguides deep in a volume using Bessel beams. The method is used to fabricate waveguides in increasingly complex geometries, integrated multiport splitters, and miniaturized functional electro-optic gates.

II. GUIDING IN A BESSEL INDEX OF REFRACTION PATTERN

A Bessel beam (BB) is an interference pattern that forms from the coherent superposition of plane waves at a fixed angle with a propagation axis [20–23]. The conical distribution of wave vectors implies that each plane-wave component has the same phase velocity along the propagation axis, say, the z axis, so that no mutual phase slippage between components intervenes. The result is a localized central peak along z that does not diffract. This peak, however, is accompanied by an elaborate and extended oscillating tail structure that actually contains most of the beam power. We thus begin by addressing the basic question of if and how an index pattern that reproduces the intensity distribution of a BB, in its finite-energy Bessel Gauss realization [24], can actually guide light along the z axis. Consider, for paraxial propagation, the inhomogeneous parabolic equation

$$\partial_z A - \frac{i}{2k}\nabla_\perp^2 A = \frac{ik}{n_0}\Delta n(I)A, \tag{1}$$

*eugenio.delre@gmail.com

 © 2019 American Physical Society

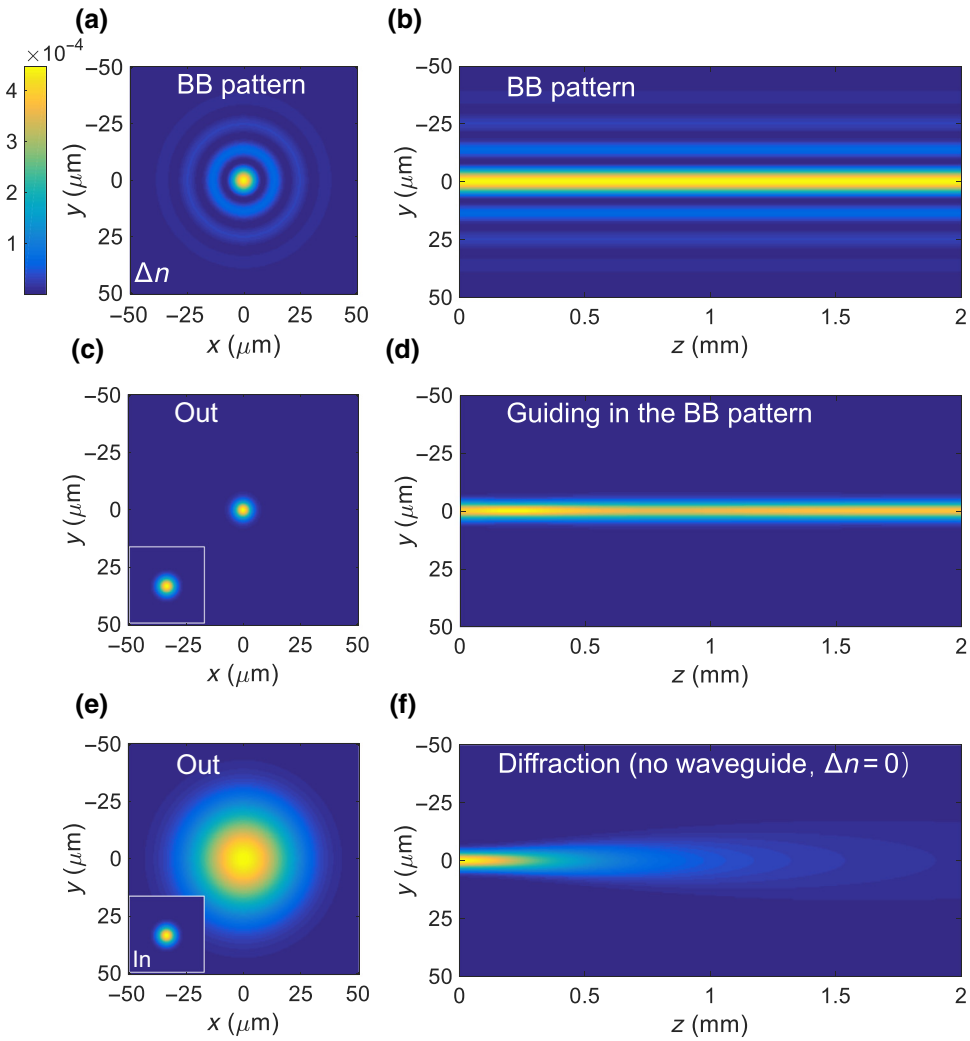

FIG. 1. A Bessel beam waveguide. (a) $\Delta n(x,y,z=0)$ and (b) $\Delta n(x=0,y,z)$ distributions for $\Delta n = \Delta n_0 |J_0(k_r r) \exp[-(r/\sigma)^2]|^2$ (BB pattern). Input and output intensity distribution (c) and propagation dynamics (d) of a Gaussian beam focused on the $z=0$ plane, i.e., $I(r,z=0) = |A_0 \exp[-(r/\sigma_G)^2]|^2$, propagating through the pattern, as predicted through a beam-propagation-method simulation [25] for $\sigma = 60$ μm, $k_r = 0.28$ μm^{-1}, $\sigma_G = 5$ μm, $\lambda = 532$ nm, and $n_0 = 2.3$. For $\Delta n_0 = 4.5 \times 10^{-4}$, the pattern is able to guide the beam that would otherwise diffract and spread for $\Delta n_0 = 0$ (e),(f).

where z is the propagation axis; (x,y) is the transverse plane; $\nabla_\perp^2 \equiv \partial_{xx}^2 + \partial_{yy}^2$; A is the slowly varying component of the optical field $E_{\rm opt} = A(r_\perp, z)\exp(-ikz)$; $k = k_0 n_0$; n_0 is the unperturbed refractive index; and $k_0 = 2\pi/\lambda$, with λ the wavelength. The index of refraction is $n = n_0 + \Delta n$, with $\Delta n = \Delta n_0 |J_0(k_r r)\exp[-(r/\sigma)^2]|^2$, where J_0 is the zeroth-order Bessel function; $r = \sqrt{x^2+y^2}$ the distance in the transverse (x,y) plane; and k_r and σ are fixed parameters [see the Bessel beam pattern in Figs. 1(a) and 1(b)]. As demonstrated in Figs. 1(c)–1(f) through a numerical simulation of Eq. (1), the z-independent BB pattern will guide a naturally diffracting Gaussian beam focused on its input plane [i.e., $A(r,z=0) = A_0 \exp[-(r/\sigma_G)^2]$] for a specific value of Δn_0.

III. EXPERIMENTS: WAVEGUIDING MECHANISM

We optically induce the BB pattern in a photorefractive crystal. Writing is carried out using a Bessel-Gauss beam with $A_w = A_{w0} J_0(k_r r)\exp[-(r/\sigma)^2]$, with k_r and σ chosen so that the Rayleigh length $z_R = \pi n \sigma^2/\lambda \gg L_z$ and the diffraction-free distance $z_D = \sigma/(k_r/k) \gg L_z$ [20], where L_z is the length of the sample along the propagation axis [24]. The photoexcitation of deep in-band impurities and charge transport leads to the formation of an optically induced space-charge field $E_{\rm sc}(I_w,t)$ given by [26]

$$E_{\rm sc}(I_w,t) = E_{0w}\left(e^{-\left(1+\frac{I_w}{I_d}\right)\frac{t}{t_d}} - 1\right). \qquad (2)$$

Here, $I_w = |A_w|^2$ is the writing intensity distribution, t is the duration of writing process, I_d and t_d are constants: the dark illumination (that can be changed by also illuminating the sample with a plane wave) and the dielectric relaxation time, respectively [26]. $E_0 = E_{0w}$ is, in turn, the constant external bias field applied to the sample along one transverse axis, say, the x axis, during the writing phase. The electric field $E = E_{0w} + E_{\rm sc}$ now changes locally the sample index of refraction through the electro-optic effect. Since the sample is heated above its room-temperature Curie point T_C, in the

paraelectric phase, it manifests a quadratic electro-optic effect according to which $\Delta n = -(1/2)n_0^3 g_{\text{eff}}\epsilon_0^2[\epsilon_r(T) - 1]^2 E^2 \equiv -\Delta n_{0,T}(E/E_0)^2$. Here, g_{eff} is the effective electro-optic coefficient, ϵ_0 is the vacuum dielectric constant, $\epsilon_r(T)$ is the low-frequency sample relative dielectric constant at the writing temperature T, and $\Delta n_{0,T} \equiv (1/2)n_0^3 g_{\text{eff}}\epsilon_0^2[\epsilon_r(T) - 1]^2 E_0^2$ is the characteristic scale of the response for the given temperature and bias field E_0. The presence of the dielectric anomaly at $T = T_C$ implies that the dielectric constant in the paraelectric phase is strongly temperature dependent, following the Curie-Weiss law $\epsilon_r(T) = C/(T - T_C)$ [27]. Hence, heating the sample to a sufficiently high temperature $T_w > T_C$ causes the electro-optic response to drop and renders nonlinear beam effects and self-writing negligible [23,28,29].

The light-induced E_{sc} of Eq. (2) can now be used as a blueprint for the electro-optic activation of a waveguide. Electro-optic activation is achieved by cooling the sample closer to the Curie point to T_g ($T_g < T_w$), leading to a strongly enhanced $\epsilon_r(T_g) > \epsilon_r(T_w)$, and applying an appropriate bias guiding electric field $E_0 = E_{0g}$. The resulting index pattern is

$$\Delta n(E_{0g}) = -(1/2)n_0^3 g_{\text{eff}}\epsilon_0^2[\epsilon_r(T_g) - 1]^2(E_{0g} + E_{\text{sc}})^2. \quad (3)$$

This index pattern can be used to guide and route an optical field A_g [Eq. (1)] with no further light-induced changes in E_{sc}. Guiding and routing can be achieved either using attenuated light ($I_g \equiv |A_g|^2 \ll I_w$), effectively halting the build-up process, or using longer-wavelength light, for which the photoexcitation process becomes

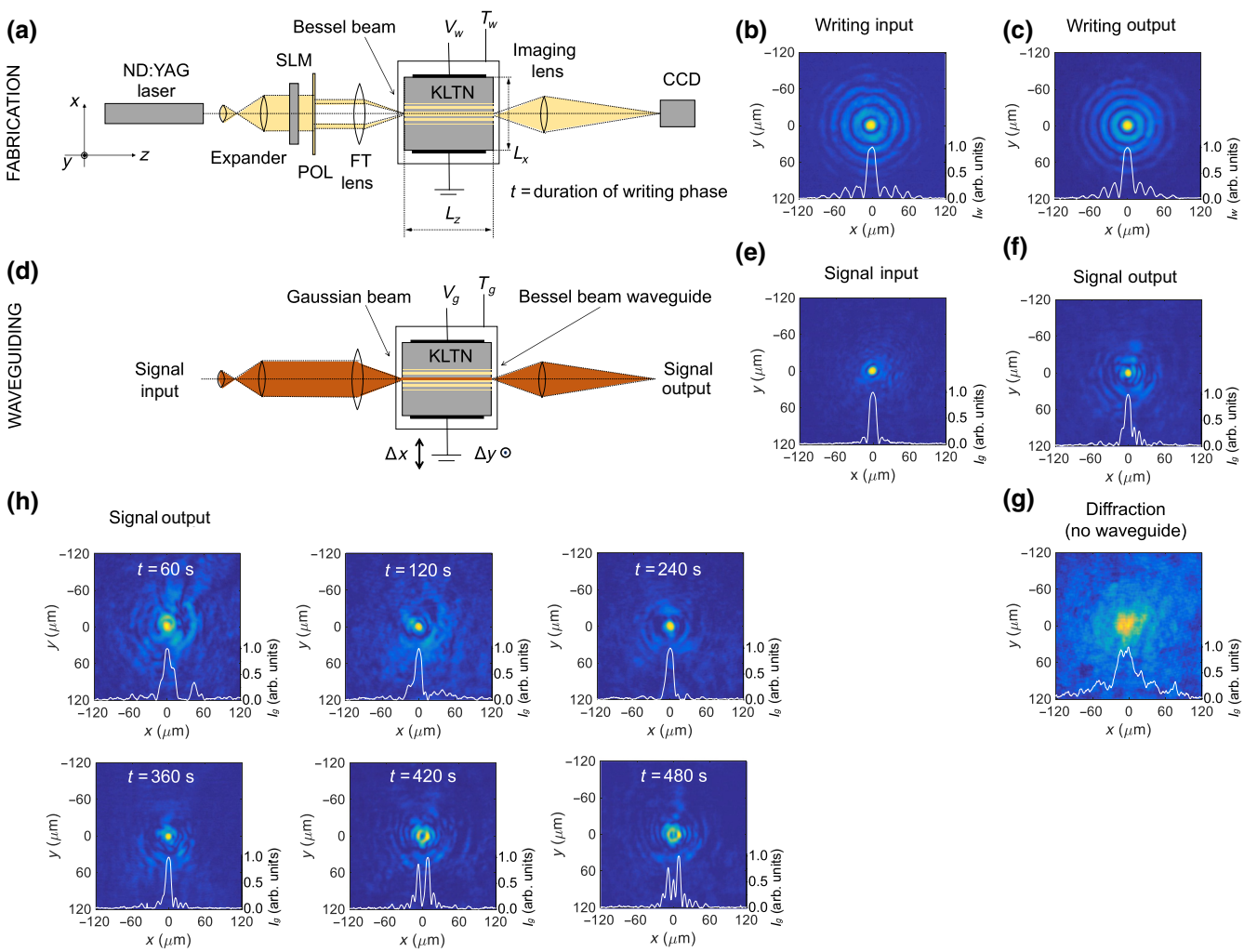

FIG. 2. Demonstration of a BB waveguide in photorefractive KLTN. Fabrication: (a) scheme of the optical writing stage; (b) input and (c) output intensity distribution of the writing beam ($k_r = 0.16\ \mu\text{m}^{-1}$ and $\sigma = 110\ \mu$m). Waveguiding: (d) scheme of the optical guiding stage; (e) input and (f) output of a Gaussian guided beam (input FWHM $= 12\ \mu$m, $\sigma_G = 10\ \mu$m) compared to (g) the diffracted output distribution with no waveguide (output FWHM $= 39\ \mu$m). Output intensity distribution (h) for different durations of the writing phase. Optimal guiding arises for $t = 240$–360 s (see panels $t = 240, 360$ s), while saturation introduces distortions for long exposure times (see panels $t = 420, 480$ s).

inefficient. For $E_{0g} = E_{0w}$ and for unsaturated conditions (i.e., $t \ll t_d$), Eqs. (2) and (3) give $\Delta n \propto I_w$, reproducing the process analyzed in Fig. 1 {with $A_g(r, z = 0) = A_0 \exp[-(r/\sigma_G)^2]$}. More generally, $E_{0g} \neq E_{0w}$ leads to a varied family of different guiding, routing, and antiguiding structures described by Eqs. (1) and (3). This allows fast electro-optic control of the index of refraction pattern with no nonlinear propagation and without involving the slow charge migration processes required to alter the space-charge density [30–32].

Experiments are carried out in a compositionally disordered photorefractive potassium-lithium-tantalate-niobate (KLTN) crystal ($K_{0.95}Li_{0.05}Ta_{0.60}Nb_{0.40}O_3$) with the setup illustrated in Fig. 2(a). The crystal is grown through the top-seeded solution method by extracting a zero-cut optical quality specimen that measures $L_x = 2.6$ mm, $L_y = 3.4$ mm, and $L_z = 1.8$ mm along the x-y-z axes. During fabrication of the waveguides, the sample is kept at $T_w = T_C + 20$ K above its ferroelectric Curie point at $T_C = 292$ K using a Peltier cell. The sample manifests a quadratic electro-optic effect with $n_0 = 2.3$, $g_{\text{eff}} = 0.14\,\text{m}^4\,\text{C}^{-2}$, and $\epsilon_r(T_w) \simeq 0.45 \times 10^4$. The bias field is obtained applying the voltage V_w to the x facets, L_x apart, so that during this stage $E_{0w} = V_w/L_x = 1.7$ kV/cm. In these conditions, the characteristic scale of the electro-optic response is $\Delta n_0 \simeq 0.4 \times 10^{-4}$, appropriately low to not affect the propagation of the writing field A_w [33,34]. There are numerous ways of generating a BB from a standard Gaussian laser beam [21,35,36]. In our experiment, a continuous-wave $\lambda = 532$ nm frequency-doubled Nd:YAG laser is enlarged and made to propagate through a spatial-light modulator (SLM) that is programmed with an intensity mask that transmits a ring. Light is then focused by a lens onto the sample, forming the BB. The A_w is then an x-polarized zeroth-order Bessel-Gauss beam with $k_r = 0.16\ \mu\text{m}^{-1}$ and $\sigma = 110\ \mu$m that is launched into the sample along the z axis. The input and output intensity distribution in the transverse (x,y) plane are imaged onto a CCD camera and reported in Figs. 2(b) and 2(c), respectively. As expected, negligible diffractive distortion is observed

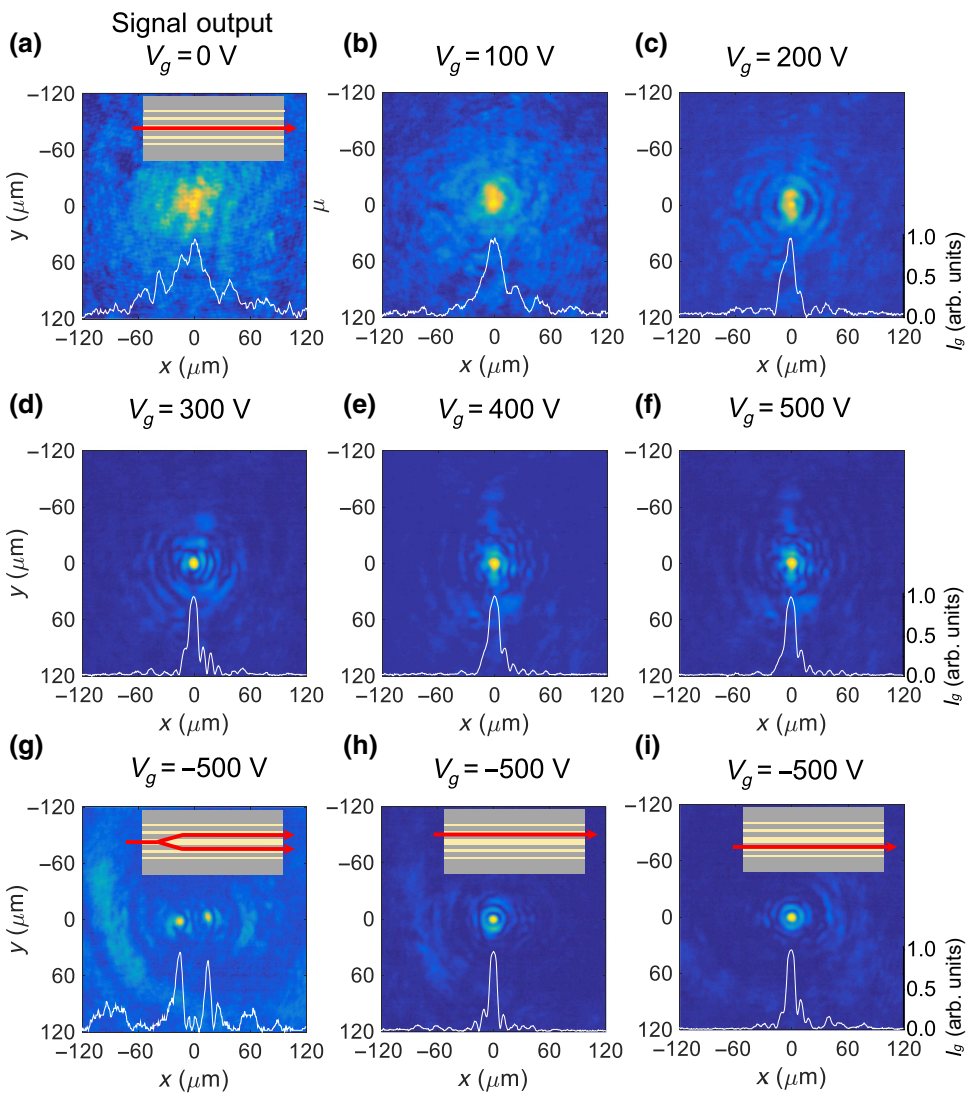

FIG. 3. Electroactivating the BB waveguide. (a)–(f) Output signal for different values of $V_g = 0$–500 V (for $V_w = 450$ V, $t = 360$ s). (g)–(i) Double waveguide structure for $(V_g/V_w) < 0$. Launching the input signal with $\Delta x = \Delta y = 0$ causes it to scatter and, in part, to be trapped into two parallel beams (g), while each is found to operate as a single waveguide by shifting the sample of $\Delta x = 9\ \mu$m (h) and $\Delta x = -9\ \mu$m (i), respectively.

for the $L_z = 1.8$ mm propagation through the sample. For a specific fabrication stage with a writing beam total input power of 1.1 μW and for an exposure time of $t = 360$ s, the waveguiding effect is reported in Figs. 2(d)–2(g). In the waveguiding stage, illustrated in Fig. 2(d), $T_g = T_C + 6$ K leads to a higher $\epsilon_r(T_g) \simeq 1.5 \times 10^4$, so that for a waveguiding bias of $E_{0g} = V_g/L_x = 1.2$ kV/cm the characteristic amplitude of the index modulation $\Delta n_0 \simeq 2 \times 10^{-4}$ can now strongly affect diffraction. Figs. 2(e)–2(g) reports the waveguiding of an input-focused 40-nW Gaussian beam (so that the ratio of the peak intensities is $I_g/I_w \simeq 0.07$) [Fig. 2(e)] that is trapped to its input 12 μm full width at half maximum (FWHM) at the output [Fig. 2(f)]. For comparison, in Fig. 2(g), we report the same output intensity distribution if no fabrication stage is enacted and the BB waveguide is absent, where the beam spreads to an output FWHM of 39 μm. As described in the model of Eqs. (2) and (3), for a given I_w, the peak index modulation and shape of the light-induced waveguide also depend on the writing exposure time t, ultimately undergoing complete saturation for $t \gg t_d$. In our specific case of peak $I_w(0,0) \simeq 0.7$ W/cm^2, the transverse output intensity distribution $I_g = |A_g(x,y,z = L_z)|^2$ for increasing values of t is reported in Fig. 2(h). For $V_w = 450$ V and $V_g = 300$ V, optimal guiding is achieved for $t = 240$–360 s. We note that each fabricated waveguide can be optically erased using a plane-wave illumination at T_w with an erasure time that is inversely proportional to the erasing intensity, allowing the optical reprogramming of the guiding structures. In our case, a BB waveguide will be completely erased by a low-intensity average 3 mW/cm^2 plane-wave illumination at T_w after 15 h.

IV. EXPERIMENTS: ELECTRO-OPTIC CONTROL

In Fig. 3, we demonstrate the electro-optic control of a single BB waveguide. The output intensity distribution for a fixed T_g and a fixed A_g is found to strongly depend on V_g ($E_{0g} = V_g/L_x$), indicating that the guiding properties of the single waveguide can be activated through an external electric signal. For the present case of $V_w = 450$ V; peak $I_w(x,y,z = L_z)$; and $t = 360$ s, optimal waveguiding is achieved for $V_g = 300$–500 V [Figs. 3(d)–3(f)].

Interestingly, the simplified model of Eq. (2) does not capture all the details of the physical processes that intervene during the writing stage. Principal among these is the intrinsic anisotropy in the space charge, associated to the fact that while the writing intensity distribution I_w is approximately circular symmetric with respect to the propagation axis z, the external electric bias is delivered through parallel plates on the x facets of the sample [26]. For $V_g < 0$, the pattern changes into two parallel and laterally shifted waveguides, in agreement with previous experiments on soliton waveguides [37]. As reported in Fig. 3(g), an input beam launched in the position of the original BB waveguide is found to scatter and partially split, guided by the two waveguides. As reported in Figs. 3(h) and 3(i), each single lateral waveguide is able to guide light independently.

V. EXPERIMENTS: MULTIPLE WAVEGUIDES AND BEAM-SPLITTERS

In Fig. 4, we demonstrate the ability to write different structures independently in the same sample in close proximity. In our specific demonstration, we fabricate two parallel waveguides at different distances. For a larger interwaveguide distance of 20 μm, each waveguide acts independently and no mode coupling is detected for the length of the sample L_z [Figs. 4(a) and 4(b)]. For a distance of 15 μm, mode coupling intervenes, and the waveguide pair acts as a more elaborate mutual phase-dependent directional coupler [Figs. 4(c)–4(e)].

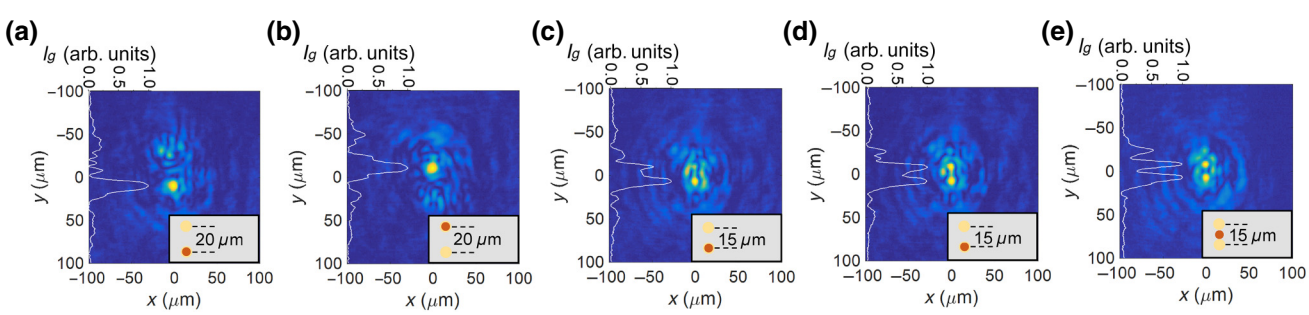

FIG. 4. Coupling between two closely packed parallel BB waveguides. Output signal intensity distribution for waveguides that are 20 μm apart when the signal input is launched into the first BB waveguide (a) with $\Delta y = 10$ μm and into the second (b) with $\Delta y = -10$ μm. For our $L_z = 1.8$ mm sample, coupling between waveguides is found to be negligible. Reducing the interwaveguide distance now leads to coupling as shown in (c),(d), where the same experiment is performed for waveguides that are 15 μm apart ($\Delta y = 7.5$ μm). Slight changes in T_g and V_g cause different coupling efficiency, as expected for directional coupling [(c),(d) are taken with $\Delta T_g \simeq 0.5$ K]. (e) Output intensity distribution when the signal input is launched in between the two waveguides ($\Delta y = 0$). In the insets, yellow points represent the BB waveguides, while red points indicate the input position of the signal Gaussian beam.

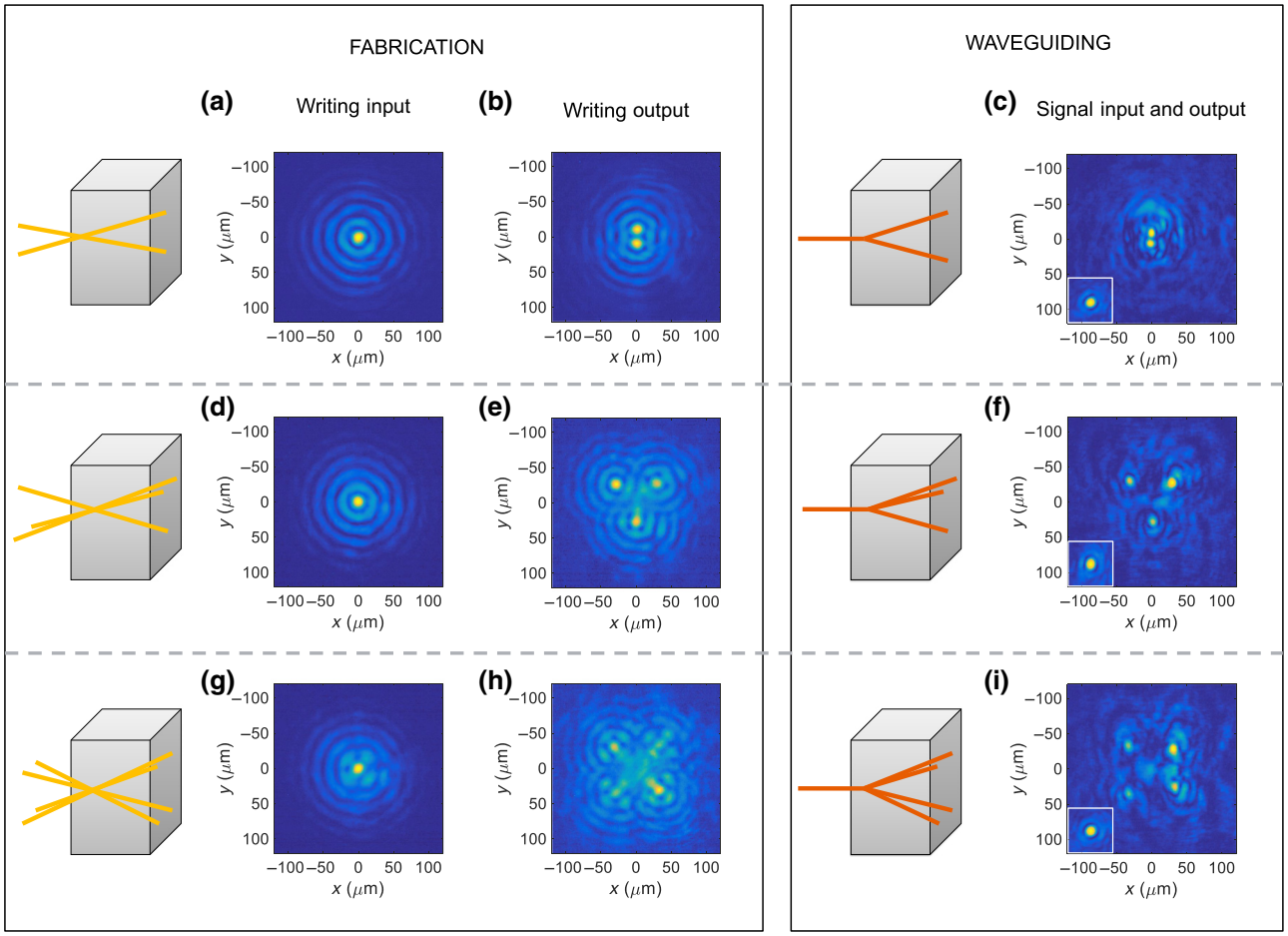

FIG. 5. Multiwaveguide structures. Left: Fabrication of a 1 × 2 (top), 1 × 3 (center), and 1 × 4 (bottom) splitter. 1 × 2: (a) Input and (b) output intensity distributions of an incoherent superposition of two BBs with a mutual angle of 8.9 mrad. Fabrication writing input and output intensity distributions for the 1 × 3 (d),(e) and 1 × 4 (g),(h) structures, where three and four incoherent BBs are launched at the input forming splitters with angles of 33.6 and 35 mrad inside of the crystal, respectively. Right: Output intensity distribution indicating the splitting of an input launch Gaussian beam at the center of the multibeam pattern (see inset) for the 1 × 2 (c), 1 × 3 (f), and 1 × 4 (i) structures.

In Fig. 5, we demonstrate the use of BB waveguide writing to achieve 1 × 2, 1 × 3, and 1 × 4 splitters launching multiple angled BBs during the fabrication stage. The BBs are rendered mutually incoherent using a specific SLM time-sequenced mask that turns on one BB at a time. This demonstrates how fabrication of complex circuitry can also be achieved in a single illumination stage without having to mechanically shift and move the sample, as instead is required in direct writing scanning techniques.

VI. CONCLUSIONS

Previous studies have made use of diffraction-free Bessel beams to guide particles and atoms and for material processing [38–44]. In this paper, we demonstrate the use of single and multiple Bessel beams to optically write waveguides and electro-optic circuits in a bulk crystal. Our method is the first scalable method to realize reprogrammable optical networks in a full 3D setting.

ACKNOWLEDGMENTS

We acknowledge support from the Lazio Innova 2018 Project (No. F83G17000850007); Sapienza-Ricerca di Ateneo 2016 and 2017 projects (No. RM116154CDA0 E195, No. RM11715C3FA0E680, and No. AR11715C808 A65EE); the H2020 Fet project PhoQus; the Doctoral Foundation of Tianjin Normal University (Grant No. 135202XB1607); and the Research and Visiting Abroad Project for Young Scholars of Tianjin Normal University 2015–2020.

[1] D. A. B. Miller, Meshing optics with applications, Nat. Photon. **11**, 403 (2017).

[2] Y. Shen, N. C. Harris, S. Skirlo, M. Prabhu, T. Baehr-Jones, M. Hochberg, X. Sun, S. Zhao, H. Larochelle, D. Englund, and M. Soljačić, Deep learning with coherent nanophotonic circuits, Nat. Photonics **11**, 441 (2017).

[3] N. C. Harris, G. R. Steinbrecher, M. Prabhu, Y Lahini, J. Mower, D. Bunandar, C. Chen, F. N. C. Wong, T. Baehr-Jones, M. Hochberg, S. Lloyd, and D. Englund, Quantum transport simulations in a programmable nanophotonic processor, Nat. Photonics **11**, 447 (2017).

[4] X. Qiang, X. Zhou, J. Wang, C. M. Wilkes, T. Loke, S. O'Gara, L. Kling, G. D. Marshall, R. Santagati, T. C. Ralph, J. B. Wang, J. L. O'Brien, M. G. Thompson, and J. C. F. Matthews, Large-scale silicon quantum photonics implementing arbitrary two-qubit processing, Nat. Photonics **12**, 534 (2018).

[5] J. W. Chan, T. R. Huser, S. H. Risbud, J. S. Hayden, and D. M. Krol, Waveguide fabrication in phosphate glasses using femtosecond laser pulses, Appl. Phys. Lett. **82**, 2371 (2003).

[6] A. C. Sullivan, M. W. Grabowski, and R. R. McLeod, Three-dimensional direct-write lithography into photopolymer, Appl. Opt. **46**, 295 (2006).

[7] G. D. Marshall, A. Politi, J. C. F. Matthews, P. Dekker, M. Ams, M. J. Withford, and J. L. O'Brien, Laser written waveguide photonic quantum circuits, Opt. Express **17**, 12546 (2009).

[8] F. Flamini, L. Magrini, A. S Rab, N. Spagnolo, V. D'Ambrosio, P. Mataloni, F. Sciarrino, T. Zandrini, A. Crespi, R. Ramponi, and R. Osellame, Thermally reconfigurable quantum photonic circuits at telecom wavelength by femtosecond laser micromachining, Light: Sci. Appl. **4**, e354 (2015).

[9] Z. Chaboyer, A. Stokes, J. Downes, M. J. Steel, and M. J. Withford, Design and fabrication of reconfigurable laser-written waveguide circuits, Opt. Express **26**, 33056 (2017).

[10] Y. Yang, X. Song, X. Li, Z. Chen, C. Zhou, Q. Zhou, and Y. Chen, Recent progress in biomimetic additive manufacturing technology: From materials to functional structures, Adv. Mater. **30**, 1706539 (2018).

[11] T. M. Monro, C. M. De Sterke, and L. Poladian, Catching light in its own trap, J. Mod. Opt. **48**, 191 (2001).

[12] M. Asaro, M. Sheldon, Z. Chen, O. Ostroverkhova, and W. E. Moerner, Soliton-induced waveguides in an organic photorefractive glass, Opt. Lett. **30**, 519 (2005).

[13] H. Terasawa, F. Tan, O. Sugihara, A. Kawasaki, D. Inoue, T. Yamashita, M. Kagami, O. Maury, Y. Bretonniere, and C. Andraud, Light-induced self-written waveguide fabrication using 1550 nm laser light, Opt. Lett. **42**, 2236 (2017).

[14] A. Bezryadina, T. Hansson, R. Gautam, B. Wetzel, G. Siggins, A. Kalmbach, J. Lamstein, D. Gallardo, E. J. Carpenter, A. Ichimura, R. Morandotti, and Z. Chen, Nonlinear Self-action of Light through Biological Suspensions, Phys. Rev. Lett. **119**, 058101 (2017).

[15] R. Malallah, D. Cassidy, I. Muniraj, J. P. Ryle, J. J. Healy, and J. T. Sheridan, Self-written waveguides in photopolymer, Appl. Opt. **57**(22), E80 (2018).

[16] S. Lan, E. DelRe, Z. Chen, M. Shih, and M. Segev, Directional coupler with soliton-induced waveguides, Opt. Lett. **24**, 475 (1999).

[17] K. Dorkenoo, O. Cregut, L. Mager, F. Gillot, C. Carre, and A. Fort, Quasi-solitonic behavior of self-written waveguides created by photopolymerization, Opt. Lett. **27**, 1499 (2002).

[18] Z. Chen, M. Segev, and D. N Christodoulides, Optical spatial solitons: Historical overview and recent advances, Rep. Prog. Phys. **75**, 086401 (2012).

[19] C. Jeng, Y. Su, R. Hong, and R. Lee, Control modulation instability in photorefractive crystals by the intensity ratio of background to signal fields, Opt. Express **23**, 10266 (2015).

[20] J. Durnin, J. J. Miceli, Jr., and J. H. Eberly, Diffraction-free Beams, Phys. Rev. Lett. **58**, 1499 (1987).

[21] D. McGloin and K. Dholakia, Bessel beams: Diffraction in a new light, Contemp. Phys. **46**, 15 (2005).

[22] L. Thibon, L. E. Lorenzo, M. Piché, and Y. D. Koninck, Resolution enhancement in confocal microscopy using Bessel-Gauss beams, Opt. Express **25**, 2162 (2017).

[23] M. Flammini, G. D. Domenico, D. Pierangeli, F. D. Mei, A. J. Agranat, and E. DelRe, Observation of Bessel-beam self-trapping, Phys. Rev. A **98**, 033808 (2018).

[24] F. Gori, G. Guattari, and C. Padovani, Bessel-gauss beams, Opt. Commun. **64**, 491 (1987).

[25] C. R. Pollock and M. Lipson, *Intergrated Photonics* (Springer, New York, 2003).

[26] E. DelRe, B. Crosignani, and P. Di Porto, Photorefractive solitons and their underlying nonlocal physics, Prog. Optics **53**, 153 (2009).

[27] E. DelRe, B. Crosignani, M. Tamburrini, M. Segev, M. Mitchell, E. Refaeli, and A. J. Agranat, One-dimensional steady-state photorefractive spatial solitons in centrosymmetric paraelectric potassium lithium tantalate niobate, Opt. Lett. **23**, 421 (1998).

[28] M. A. Porras, A. Parola, D. Faccio, A. Dubietis, and P. Di Trapani, Nonlinear Unbalanced Bessel Beams: Stationary Conical Waves Supported by Nonlinear Losses, Phys. Rev. Lett. **93**, 153902 (2004).

[29] M. A. Porras, C. Ruiz-Jimenez, and J. C. Losada, Underlying conservation and stability laws in nonlinear propagation of axicon-generated Bessel beams, Phys. Rev. A **92**, 063826 (2015).

[30] E. DelRe, B. Crosignani, E. Palange, and A. J. Agranat, Electro-optic beam manipulation through photorefractive needles, Opt. Lett. **27**, 2188 (2002).

[31] A. Pierangelo, A. Ciattoni, E. Palange, A. J. Agranat, and E. DelRe, Electro-activation and electro-morphing of photorefractive funnel waveguides, Opt. Express **17**, 22659 (2009).

[32] J. Parravicini, R. Martínez Lorente, F. Di Mei, D. Pierangeli, A. J. Agranat, and E. DelRe, Volume integrated phase modulator based on funnel waveguides for reconfigurable miniaturized optical circuits, Opt. Lett. **40**, 1386 (2015).

[33] E. DelRe, A. Pierangelo, E. Palange, A. Ciattoni, and A. J. Agranat, Beam Shaping and Effective Guiding in the Bulk of Photorefractive Crystals through Linear Beam Dynamics, Appl. Phys. Lett. **91**, 081105 (2007).

[34] A. Pierangelo, E. DelRe, A. Ciattoni, E. Palange, A. J. Agranat, and B. Crosignani, Linear writing of waveguides in bulk photorefractive crystals through a two-step polarization sequence, J. Opt. A - Pure and Appl. Opt. **10**, 064005 (2008).

[35] G. Di Domenico, J. Parravicini, G. Antonacci, S. Silvestri, A. J. Agranat, and E. DelRe, Miniaturized photogenerated electro-optic axicon lens Gaussian-to-Bessel beam conversion, Appl. Opt. **56**, 2908 (2017).

[36] G. Antonacci, G. Di Domenico, S. Silvestri, E. DelRe, and G. Ruocco, Diffraction-free light droplets for axially-resolved volume imaging, Sci. Rep. **7**, 17 (2017).

[37] E. DelRe, A. Ciattoni, and A. J. Agranat, Anisotropic charge displacement supporting isolated photorefractive optical needles, Opt. Lett. **26**, 908 (2001).

[38] J. Arlt, T. Hitomi, and K. Dholakia, Atom guiding along Laguerre-Gaussian and Bessel light beams, Appl. Phys. B **71**, 549 (2000).

[39] J. Arlt, V. Garces-Chavez, W. Sibbett, and K. Dholakia, Optical micromanipulation using a Bessel light beam, Opt. Commun. **197**, 239 (2001).

[40] P. Polesana, D. Faccio, P. Di Trapani, A. Dubietis, A. Piskarskas, A. Couairon, and M. A. Porras, High localization, focal depth and contrast by means of nonlinear Bessel beams, Opt. Express **13**, 6160 (2005).

[41] V. Zambon, N. McCarthy, and M. Piché, Fabrication of photonic devices directly written in glass using ultrafast Bessel beams, Proc. SPIE **7099**, 70992J (2008).

[42] M. K. Bhuyan, F. Courvoisier, P. A. Lacourt, M. Jacquot, L. Furfaro, M. J. Withford, and J. M. Dudley, High aspect ratio taper-free microchannel fabrication using femtosecond Bessel beams, Opt. Express **18**, 566 (2010).

[43] C. L. Arnold, S. Akturk, A. Mysyrowicz, V. Jukna, A. Couairon, T. Itina, R. Stoian, C. Xie, J. M. Dudley, F. Courvoisier, S. Bonanomi, O. Jedrkiewicz, and P. Di Trapani, Nonlinear Bessel vortex beams for applications, J. Phys. B: At. Mol. Opt. Phys. **48**, 094006 (2015).

[44] C. Xie, V. Jukna, C. Milián, R. Giust, I. Ouadghiri-Idrissi, T. Itina, J. M. Dudley, A. Couairon, and F. Courvoisier, Tubular filamentation for laser material processing, Sci. Rep. **5**, 8914 (2015).